Author/s:
Yan, D;Cuevas, A;Stuckelberger, J;Wang, E-C;Phang, SP;Kho, TC;Michel, JI;Macdonald, D;Bullock, J

Title:
Silicon solar cells with passivating contacts: Classification and performance

Date:
2023-04-01

Citation:
Yan, D., Cuevas, A., Stuckelberger, J., Wang, E. -C., Phang, S. P., Kho, T. C., Michel, J. I., Macdonald, D. & Bullock, J. (2023). Silicon solar cells with passivating contacts: Classification and performance. PROGRESS IN PHOTOVOLTAICS, 31 (4), pp.310-326. https://doi.org/10.1002/pip.3574.

Persistent Link:
https://hdl.handle.net/11343/308312

Received: 27 October 2021 | Revised: 1 April 2022 | Accepted: 19 April 2022

DOI: 10.1002/pip.3574

SPECIAL ISSUE ARTICLE

PROGRESS IN PHOTOVOLTAICS WILEY

Silicon solar cells with passivating contacts: Classification and performance

Di Yan[1] | Andres Cuevas[2] | Josua Stuckelberger[2] | Er-Chien Wang[2] | Sieu Pheng Phang[2] | Teng Choon Kho[2] | Jesús Ibarra Michel[1] | Daniel Macdonald[2] | James Bullock[1]

[1]Department of Electrical and Electronic Engineering, The University of Melbourne, Melbourne, VIC, Australia

[2]School of Engineering, The Australian National University, Canberra, ACT, Australia

Correspondence
Daniel Macdonald, School of Engineering, The Australian National University, Canberra, ACT 2601, Australia.
Email: daniel.macdonald@anu.edu.au

James Bullock, Department of Electrical and Electronic Engineering, The University of Melbourne, Victoria 3010, Australia.
Email: james.bullock@unimelb.edu.au

Funding information
Australian Centre for Advanced Photovoltaics; Australian Renewable Energy Agency

Abstract

The year 2014 marks the point when silicon solar cells surpassed the 25% efficiency mark. Since then, all devices exceeding this mark, both small and large area, with contacts on both sides of the silicon wafer or just at the back, have utilized at least one passivating contact. Here, a passivating contact is defined as a group of layers that simultaneously provide selective conduction of charge carriers and effective passivation of the silicon surface. The widespread success of passivating contacts has prompted increased research into ways in which carrier-selective junctions can be formed, yielding a diverse range of approaches. This paper seeks to classify passivating contact solar cells into three families, according to the material used for charge-carrier selection: doped amorphous silicon, doped polycrystalline silicon, and metal compounds/organic materials. The paper tabulates their current efficiency values, discusses distinctive features, advantages, and limitations, and highlights promising opportunities going forth towards even higher conversion efficiencies.

KEYWORDS
heterojunction, metal compounds, passivating contacts, polysilicon contacts, silicon solar cells

1 | INTRODUCTION TO PASSIVATING CONTACTS, OR JUNCTIONS

In state of the art, mass-produced silicon solar cells, thin layers of transparent dielectric materials like SiO_x, AlO_x, and SiN_x are deposited on the front and back surfaces to reduce electron–hole recombination, except for a small portion, a mere 1–4%, where the metal electrodes make contact with n^+ and p^+ regions formed by diffusing or alloying/recrystallizing dopants into the silicon wafer (see Figure 1).[1] Although those n^+ and p^+ regions help to reduce it, finding more effective ways to suppress recombination at the metal/semiconductor interfaces, that is, to passivate them, has become essential for silicon solar cells to reach their full potential. One possibility is to extend the passivation layer underneath the metal electrodes, and this has been demonstrated with SiO_x,[2] AlO_x,[3] or a-Si(i):H[4] on top of a phosphorus diffusion. Nevertheless, such an approach has its own limitations and has not found widespread adoption.

The so-called "passivating contacts," or "passivated contacts,"[5–7] intend to go further, seeking to suppress recombination related, not just to the metal/semiconductor interface, but to the whole junction. Here, the junction refers to the layer or layers that when deposited on, or formed in, the silicon wafer serve to separate electrons from holes, selecting one charge carrier type for transport towards one of the metal electrodes while hindering the other carrier. In the broad

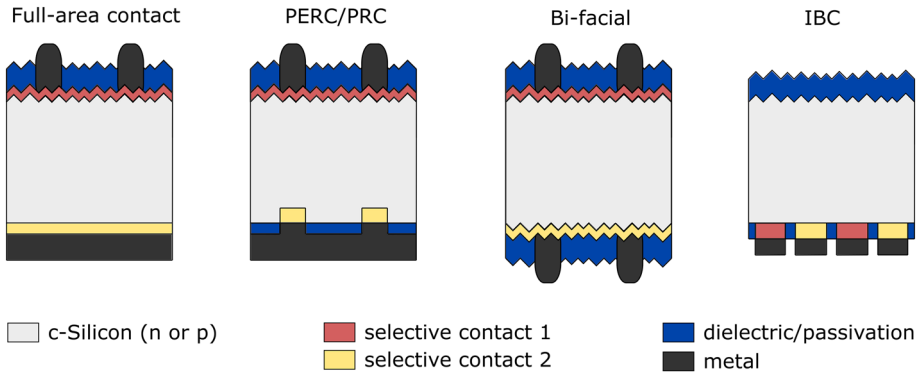

FIGURE 1 Four common silicon solar cells implemented with carrier selective contacts, from left to right, both sided contact silicon solar cells with rear full-area contact (full-area contact), both sided contact silicon solar cells with partial rear contacts (PERC/PRC), bifacial silicon solar cells with both sided contacts (Bi-facial), and interdigitated back contact cells (IBC)

sense, therefore, a "passivating contact," which may appropriately be called a "passivating junction," encompasses several of the functions necessary for the efficient operation of a solar cell device: passivate surfaces and interfaces, provide a high conductivity for just one type of charge carrier, and establish a bridge between the work functions of silicon and silver or aluminum, the metals commonly used to form the electrodes. In practice, most passivating contact structures are composed of several layers, specialized for each of those functions. For example, in the well-known silicon heterojunction (SHJ) technology, an intrinsic hydrogenated amorphous silicon layer provides passivation of the Si wafer absorber, a doped a-Si:H layer provides good vertical conductivity and a suitable work function for carrier selection, and a well-designed transparent conductive oxide (TCO) reduces sensitivity to the work function of the metallic terminals, in addition to providing lateral current transport and light coupling.[8]

As in the case of the SHJ, most passivated contact structures include a passivating layer at the interface with the silicon wafer, buried underneath other layers, and this means that it must permit the passage of electric current.[9] The materials that best passivate silicon surfaces are poor conductors like a-Si(i):H, or insulators like SiO_x, and hence their addition typically increases the resistance of the contact structure. The compromise between passivation and transport depends on the extent of the surface that is contacted; for small area contacts (i.e., 1–4% surface coverage) the passivation layer is made very thin to achieve a low contact resistivity; and for large/full-area contacts, a thicker and better passivating film is preferable, because a higher contact resistivity can be tolerated. Therefore, the geometrical design of the solar cell is another tool that can be used to best utilize the strengths of a given passivating contact structure or technology.

High-quality passivation generally involves the participation of atomic hydrogen to reduce the density of interface defects, either as part of the passivating material, as is the case of a-Si(i):H, or incorporated by means of a dedicated hydrogenation treatment, for instance by depositing capping layers, such as the common antireflection layer of SiN_x:H, and annealing them to release hydrogen. It is important to remember, though, that surface and contact recombination can be reduced not only by the chemical bonding of appropriate atoms like H, O or Si, but also by manipulating the population of charge carriers near the surface.[10] A large asymmetry between the concentrations of electrons and holes typically results in a lower probability that they recombine via the Shockley–Read–Hall (SRH) mechanism, as long as the concentration of one of the two does not become high enough to trigger other mechanisms, like Auger recombination. Carrier population control is almost always part of the surface and contact passivation techniques, either via fixed charges in a deposited dielectric layer, the work function of the materials used (including both those that form the passivating contact structure and the metal electrodes), the doping of the near-surface silicon region, or a combination of those factors; moreover, it is particularly relevant for passivated contact structures, tasked with the function of conducting just one of the two carriers. A high concentration of one carrier type automatically confers silicon a high conductivity for that carrier and a low conductivity for the other carrier; that is, it provides carrier selectivity.[11] It is therefore sensible that attention be paid to choosing the materials that compose a passivating contact structure so that at least one of them has a very low (for electron selection) or very high (for hole selection) work function. Note that the work function of Si and a-Si:H can be modified by doping to make it either low (n-type) or high (p-type).

A nearly zero recombination rate and a low enough resistance are two features of what we could call an "ideal" carrier-selective junction (or contact), but they are not the only ones. A high transparency/low photon absorption is also necessary, especially when the junction is placed on the front surface, but also at the back, particularly if the solar cell is intended for albedo collection. Photon absorption within the carrier-selective material is only tolerable if its electronic quality is good enough to permit the transport of minority carriers, so that they can flow out of it before recombining. This is possible for dopant-diffused monocrystalline silicon, but it is problematic for most materials used to make passivating contact structures, which requires that they are made very thin to limit absorption losses. Another aspect to consider is that in most cases the junction/contact structure needs to provide a low-resistance lateral pathway towards the metal grid for the majority carriers (i.e., the carriers selected by that junction). Again, crystalline silicon can do that well, but other contact systems, like those based on a-Si:H, need to be complemented with a conductive layer, usually a TCO. The most common is indium-tin oxide (ITO), which can have a high conductivity, although at the expense of slightly reducing its transparency.

There are quite a few materials that can be used as carrier-selective conductors and there are different ways in which they can be combined with passivating layers. In this paper, we have classified the diversity of passivating contact structures reported so far in three families, according to the material used to perform the main function of the contact/junction, which is the selective conduction of one type of charge carrier. To give an overview of the state of the art, we emphasize cell-level demonstrations, compiling the most impressive results to date in the form of efficiency tables. We start with the SHJ solar cells, based on the selective conduction of doped amorphous silicon (Section 2), which have achieved the highest levels of performance and therefore serves as a benchmark. The second family (Section 3) is based on the selective conduction of doped polycrystalline silicon (poly-Si), which combined with an ultrathin layer of SiO_x, can provide a similar level of passivation as the SHJ. Finally, in a third family (Section 4) we group all the contact/junction systems that, rather than employing doped silicon films, utilize the natural work function and/or selective conductivity of various metal compounds and organic materials. Most of the solar cells presented in Sections 3 and 4 are hybrid devices, that is, with each of the two carrier-selective junctions belonging to a different family. The scope of this article is to document the current cell-level performance of the three main passivating contact technologies. More details on the intricacies of each of these passivating contact technologies is discussed extensively in other articles within this special issue on passivating contacts based silicon solar cells. For example, Zhao et al. present strategies to improve the performance of SHJ solar cells[12]; Glunz et al. present an overview of the historical development of poly-Si passivating contacts and their current status in both industry and research laboratories[5]; Singh et al. and Nandakumar et al. focus on the industrial aspects of poly-Si passivating contacts,[13,14]; and Ibarra Michel et al. review metal compound-based passivating contacts.[15]

Each efficiency table is composed of three parts. The first part describes the architecture of the solar cell, including its front and rear contact/junction structures, and the type of silicon wafer used; for Section 4, we also include the geometry of the passivating contact and relevant material properties. The central part of the tables gives the main performance parameters, as well as the area and thickness of the solar cell. The last part indicates the performance certification and year, if available, the institution/authorship for each device, and a reference. As mentioned above, a given junction/contact does not need to cover the whole surface of the solar cell. Geometrical restriction of the contact area can be very effective with material systems that cannot achieve good passivation, as long as their contact resistivity is low. In Section 4, we also include examples of devices with a partial rear contact based on functional materials that possess either a very low (e.g., LiF_x/Al) or very high (e.g., MoO_x) work function. Contact patterning is, of course, also necessary to make interdigitated back contact cells (IBC) with any of the technologies discussed in this paper, even though in that case the sum of both carrier-selective contacts usually covers a large fraction of the cells' rear surface.

2 | SHJ SOLAR CELLS

SHJ solar cells were the first reported high efficiency crystalline silicon cell structures using a wider bandgap "passivating contact." In particular, this structure employed stacks of intrinsic and doped hydrogenated amorphous silicon (a-Si:H) layers, for both contacts of the solar cell. The intrinsic a-Si:H layer can provide excellent chemical passivation whereas the doped a-S:H layer provides carrier selectivity. The role of a-Si:H as a passivation and junction building layer for crystalline silicon was reported already in the 1970s,[16,17] while the first solar cell devices were pioneered in the late 1980s and the 1990s by Sanyo (now part of Panasonic) under the trademark Hetero Intrinsic Thin layer (HIT).[18,19] The excellent surface passivating performance, capable of enabling open circuit voltages of 740 to 750 mV,[20] the high efficiency, small temperature coefficients,[21,22] and production simplicity, have attracted the attention of both industry and research institutes. However, SHJ solar cells are not without limitations. First, the a-Si:H layers start to deteriorate above 300°C, which is very different to most of the other silicon solar cell architectures involving thermal diffusion of dopants for junction formation. This means that any process steps after the a-Si:H passivating contact formation must be below 300°C. A most direct result of this is the necessity of non-fire-through metallization, requiring a dedicated low-temperature metal paste, which is more expensive. Second, due to the low lateral conductivity of the a-Si:H layers, a TCO layer is necessary on top of the a-Si:H stack for lateral carrier transport, work function alignment as well as antireflection. Additionally, there is a non-negligible vertical contact resistivity through the a-Si:H stack. Lastly, both the TCO and the a-Si:H stack absorb light parasitically in the entire spectrum of interest, especially in the short wavelength range, which results in 1–2 mA/cm^2 drop in J_{SC} (short circuit current density) when compared with traditional dopant-diffused junctions.[23,24]

The devices presented in this section are summarized in Tables 1a, 1b, and 1c and have been selected based either on their outstanding performances, their specific architectures or because they incorporate distinctive and notable alteration to the layer stacks to reduce fabrication complexity or energy losses. Table 1a lists small area both sides contacted SHJ solar cells from laboratories, Table 1b lists large area both sides contacted SHJ solar cells from industries, and Table 1c lists both small and large area SHJ interdigitated back contacted (IBC) devices.

The fabrication procedure of a typical SHJ solar cell starts with wafer cleaning and alkaline texturing, followed by single-side intrinsic and doped a-Si:H stack formation (usually the junction side first, e.g., a-Si(i):H/a-Si(p):H for n-type Si substrates) by plasma enhanced chemical vapor deposition (PECVD), and then the opposite polarity on the other side, for example, a-Si(i):H/a-Si(n):H for n-type Si substrates. Next, a TCO layer applied by physical vapor deposition (PVD) caps the front and rear sides of the cell followed by metal electrode formation by PVD, screen printing, or electroplating. The process temperatures within the entire fabrication procedure are usually less than 300°C, with PECVD being the highest temperature process. Typical

TABLE 1a Small area silicon heterojunction solar cells with both sides contacted

Device structure												
No.	Front side	Substrate	Rear side	V_{OC} (mV)	J_{SC} (mA/cm^2)	*FF* (%)	Efficiency (%)	Area (cm^2)	Wafer thickness (μm)	Certification	Year	Institution
1a-1	ITO/**a-Si (n):H/ a-Si(i): H**	n-type	**a-Si(i):H/ a-Si (p):H/** ITO	730	40.3	82.3	24.2	4.0	230	CalTeC/ ISFH[a]	2019	CSEM[25]
1a-2	ITO/**nc-SiC (n)/** SiO_x	n-type	**a-Si(i):H/ a-Si (p):H/** ITO	725	40.9	80.9	24.0	3.5	170	CalTeC/ ISFH	2021	Jülich[26]
1a-3	ITO/**a-Si (n):H/ a-Si(i): H**	p-type	**a-Si(i):H/ a-Si (p):H/** ITO	723	40.7	80.8	23.8	4.0	230	CalTeC/ ISFH	2019	CSEM[25]

[a]ISFH: Institute for Solar Energy Research in Hamelin.

TABLE 1b Large area silicon heterojunction solar cells with both sides contacted

Device structure												
No.	Front side	Substrate	Rear side	V_{OC} (mV)	J_{SC} (mA/cm^2)	*FF* (%)	Efficiency (%)	Area (cm^2)	Wafer thickness (μm)	Certification	Year	Institution
1b-1	*N/A*	*N/A*	*N/A*	750	40.5	86.6	26.3	275.6	*N/A*	CalTeC/ ISFH	2021	LONGi[27]
1b-2	*N/A*	*N/A*	*N/A*	746	40.2	85.1	25.5	274.5	*N/A*	CalTeC/ ISFH	2021	Suzhou Maxwell/ SunDrive Solar[28]
1b-3	*N/A*	*N/A*	*N/A*	746	40.0	84.6	25.3	274.5	*N/A*	CalTeC/ ISFH	2021	HuaSun[29]
1b-4	ITO/ **μc-SiO_x/ a-Si(i):H**	n-type	**a-Si(i):H/ a-Si(n): H/**ITO	747	39.6	84.9	25.1	244.5	150	CalTeC/ ISFH	2020	Hanergy[30]
1b-5	TCO/ **a-Si(p):H/ a-Si(i):H**	n-type	**a-Si(i):HJ/ a-Si(n): H/**TCO	738	40.8	83.5	25.1	151.9	160	CalLab/Fh-ISE[a]	2015	Kaneka corporation[31]
1b-6	TCO/ **a-Si(p):H/ a-Si(i):H**	n-type	**a-Si(i):H/ a-Si(n): H/**TCO	750	39.5	83.2	24.7	102.0	98	AIST[b]	2013	Sanyo[20]

[a]Fh-ISE: Fraunhofer Institute for Solar Energy Systems.
[b]AIST: Advanced Industrial Science and Technology.

SHJ solar cells use high quality n-type Cz substrates to take advantage of the excellent surface passivation provided by a-Si(i):H while avoiding bulk recombination to achieve high open-circuit voltage (*device No. 1a-1*). Also, because no high temperature processes are involved, high temperature gettering of impurities is not achievable, unless performed separately.[35] Recent wafer cost estimations show that n-type Cz wafers are 10% more expensive than p-type Cz wafers.[36] This is related to the fact that n-type wafers currently make up less than 15% of the global market. However, this share is expected to increase and reach parity in 2031,[37] which in principle should result in similar production costs for n- and p-type wafers. In any case, Descoeudres et al. have shown that p-type SHJ solar cells can be comparable in efficiency if phosphorus gettering is incorporated (*device No. 1a-3*).[25]

The wider bandgap of the a-Si:H layer, relative to c-Si, in combination with the high amount of hydrogen incorporated in a-Si:H ensures excellent surface passivation; however, it also comes with the cost of parasitic absorption. This parasitic absorption also increases when the a-Si:H is doped with impurities to achieve carrier selectivity, for which a thicker layer is generally required to achieve the desired band alignment and low contact resistivity. To overcome this, the amorphous silicon layers on the light facing side can either be nanocrystallized, oxidized,[30,38,39] or carbonized[26,40,41] to reduce parasitic absorption while maintaining high levels of surface passivation and carrier selectivity (*devices No. 1a-2* and *No. 1b-3*). Nevertheless, optimizing the TCO layer capping the a-Si:H stacks on the front and rear of SHJ solar cells still involves balancing optical transparency, electrical conductivity, and material cost.

TABLE 1c Silicon heterojunction solar cells with IBC structures

Device structure				V_{OC} (mV)	J_{SC} (mA/cm^2)	*FF* (%)	Efficiency (%)	Area (cm^2)	Wafer thickness (μm)	Certification	Year	Institution
No.	Electron contact	Substrate	Hole contact									
1c-1	**a-Si(i):H/a-Si(n):H/** Electrode	n-type	**a-Si(i):H/a-Si(p):H/** Electrode	738	42.7	84.9	26.7	79.0	N/A	AIST	2017	Kaneka corporation[32]
1c-2	**a-Si(i):H/a-Si(n):H/** Electrode	n-type	**a-Si(i):H/a-Si(p):H/** Electrode	740	41.8	82.7	25.6	143.7	150	AIST	2014	Panasonic[33]
1c-3	**a-Si(i):H/a-Si(n):H/TCO**	n-type	**a-Si(i):H/a-Si(p):H/TCO**	736	41.5	81.9	25.0	25.0	N/A	CalTeC/ ISFH	2019	CSEM[25]
1c-4	**a-Si(i):H/a-Si(n):H/TCO**	n-type	**a-Si(i):H/a-Si(p):H/TCO**	729	40.7	76.4	22.6	9.0	N/A	CalTeC/ ISFH	2017	EPFL[34]

As early as 2013, Sanyo (part of Panasonic) demonstrated a large area SHJ solar cell with a 24.7% conversion efficiency (*device No. 1b-6*).[20] As of 2021, there are several large PV companies developing SHJ solar cell technology, including LONGi Solar[27] (*device No. 1b-1*) and Risen Energy. Others are already producing them at large-scale, including Renewable Energy Corporation (REC Solar), Meyer Burger, HuaSun[29] (*device No. 1b-3*), Hanergy[30] (*device No. 1b-4*), and Hevel Group. Recently LONGI has demonstrated a certified large area SHJ efficiency of 26.3% (*device No. 1b-1*). Suzhou Maxwell and SunDrive Solar (*device No. 1b-2*) have achieved a certified large area SHJ efficiency result of 25.5% utilizing a production-line compatible seedless copper plating process to create the metal electrodes.[28] The copper plating process, also used for *device 1b-5*, avoids the use of silver metal while being able to create high aspect ratio fingers, resulting in a high J_{SC}.[31] These companies seek to take advantage of the simplified fabrication procedures, high conversion efficiency, and courtesy of the high V_{OC}, a smaller drop in output power during high temperature operation (i.e., small temperature coefficient) compared with other cell technologies.

The interdigitated-back-contact (IBC) architecture is an obvious route to minimizing front parasitic absorption. In 2014, Panasonic demonstrated a large area SHJ IBC solar cell that reached a 25.6% conversion efficiency (device No. 1c-2),[33] setting a new benchmark. Since 2017, the conversion efficiency record for a silicon solar cell has been held by Kaneka corporation, using the IBC architecture SHJ solar cell, reaching 26.7% (*device No. 1c-1*).[32] Tomasi et al.[34] and Descoeudres et al.[25] demonstrated that the fabrication complexity of IBC-SHJ, as shown by *devices No. 1c-3* and *No. 1c-4*, can be reduced to just one shadow mask step during the deposition of one a-Si:H polarity, whereas the other a-Si:H polarity can simply be deposited across the entire rear surface. They demonstrated that the collection of carriers through the double polarity stacks can be achieved through an interband-tunneling mechanism.

The development of TCO layers and the metallization process for the front and rear of the SHJ solar cell is currently a focus for many groups working on this architecture. The most common TCO, indium tin oxide (ITO), has a good combination of conductivity, transparency and thermal stability. However, as with all transparent conducting films, a trade-off must be made between the conductivity and transparency due to the parasitic absorption of charge carriers. It also has the drawback of high cost due to the limited annual indium supply. Alternative solutions include replacing ITO with ZnO:Al to avoid indium entirely or adopt other indium-based TCOs with higher mobility and transparency, for example, hydrogenated indium oxide (IO:H).[24] For lower temperature silver paste, the connection between silver particles is mainly composed of organic binding agents, resulting in high porosity after curing. This is different from the traditional high temperature firing silver paste, in which silver particles are connected to each other during the sintering process. To overcome this, wider fingers and higher silver consumption are necessary.[42] A few approaches to reduce silver consumption have been proposed and demonstrated, for example, copper screen printing paste[30] and copper plating process,[28,31]

The SHJ architecture has also shown its potential in tandem configurations with other semiconductor materials. The two most recent 2-terminal perovskite–silicon tandem solar cell efficiency breakthroughs of 29.5% by Oxford PV and 29.15% by HZB both adopted SHJ front and rear contacted solar cells as the bottom sub-cell.[43,44] The high open-circuit voltage of the SHJ cell is advantageous, whereas the compromised short-circuit current density is less significant, as light in the short to mid wavelength range is already absorbed by the perovskite top cell before reaching the silicon bottom cell.

3 | SOLAR CELLS WITH POLYCRYSTALLINE SILICON PASSIVATING CONTACTS

Similar to a-Si:H-based contacts, the history of doped polysilicon passivating contacts (poly-Si) applied on silicon solar cells extends well into the past, with early studies in the 1980s.[45–50] A widespread attention came in 2013 with the results of Feldmann et al.,[51] whose demonstration of n^+ poly-Si passivating contacts on n-type Si solar cells with high fill factor and an efficiency of 23%, revived the interest in poly-Si. Thereafter, a substantial R&D effort, combined with improvements in other aspects of cell fabrication, has further pushed cell efficiencies to above 26% for small area solar cells in research institutes,[52,53] and above 25% for large area solar cells in industry.[54–56] Poly-Si passivating contacts are particularly attractive to the current PV industry due to the compatibility with the relatively high temperatures used during metallization by screen printing, and similarity of their required fabrication equipment with that currently used in production lines. This structure is commonly referred to as a tunnel oxide passivated contact (TOPCon), polycrystalline silicon on oxide (POLO) or simply as a poly-Si passivating contact.

A conventional poly-Si structure consists of an ultra-thin silicon oxide stacked with a heavily doped poly-Si layer. The three main steps in creating a poly-Si passivating contact are hence the formation of the interfacial oxide, the deposition of amorphous or polycrystalline silicon layers, and the introduction or activation of dopants of the deposited silicon layer. The thin silicon oxide layer, usually 1–2 nm thick, is required to provide excellent surface passivation while maintaining good carrier transport for the majority carriers between the doped polysilicon and the silicon bulk, either through tunneling for thinner oxide layers, or via pinholes for thicker oxide layers, or a combination of both.[57] Such thin silicon oxide layers can be formed either chemically using nitric acid, RCA 2 solution, or ozone oxidation,[58] thermally in a tube furnace at temperatures between 600°C to 800°C[47,48] or deposited using chemical vapor deposition.[59] Deposition of the poly-Si layer can be performed using either low-pressure chemical vapor deposition (LPCVD),[52,56,60] plasma-enhanced chemical vapor deposition (PECVD),[52,53] atmospheric pressure chemical vapor deposition (APCVD),[61] or physical vapor deposition (e.g., sputtering and e-beam evaporation),[62,63] If not already doped in-situ during deposition,[64,65] the polysilicon layer can be subsequently doped via ion implantation,[52] high temperature dopant diffusion,[66] or via deposition of a dopant-rich film.[67] It should be noted that a high-temperature activation anneal in an inert ambient is typically required to electrically activate the dopants,[52,64] and to crystallize the polysilicon, which can range from amorphous to polycrystalline in the as-deposited state (depending on the deposition method and conditions).[68] Hydrogenation of the SiO_x/c-Si interface,[69] either through hydrogen plasma or annealing with hydrogen rich capping layers, such as Al_2O_3 or SiN_x, is also frequently applied to further improve the surface passivation of the passivating contact.[70] Remarkably, excellent carrier selectivity has been demonstrated for most combinations of oxide growth, poly-Si deposition, and doping methods, after optimization of the processing conditions.

Recombination current density pre-factor J_0 and contact resistivity values are commonly reported to demonstrate the performance of poly-Si passivated contacts. Excellent surface passivation with J_0 values less than 10 fA/cm^2 has been demonstrated on both phosphorus doped n^+ and boron doped p^+ poly-Si, but the general trend in the literature shows higher J_0 values for p^+ polysilicon, particularly after metallization.[71] Their differences have been intensively studied with most authors attributing the diffusivity and segregation of dopants in both poly-Si layers and interfacial SiO_2 layers, as well as the interfacial layer distortion as the main points of difference. Boron can easily penetrate through the SiO_2 and enhances interface defects. Thus, controlling the amount of boron in SiO_2 is critical to improving the performance of boron doped poly-Si contacts, which can be done by modifying the poly-Si structures and interfacial layers. Alternatively, replacing Boron with other possible p-type dopants has also been demonstrated, for example, Ga, unfortunately, at the expense of a high contact resistivity. As a result, the application of doped poly-Si passivating contacts on solar cells has been mainly focused on n^+ poly-Si to date. The highest efficiency silicon solar cells with both-side-contacts are made based on n^+ poly-Si as demonstrated by FhISE. The contact resistivity for both n^+ and p^+ doped polysilicon passivating contacts can vary within the range of 0.2–100 mΩ cm^2,[28,42,58,72]

The cell results in the tables are categorized into small area both sides contacted cells (Table 2a), large area both sides contacted cells (Table 2b), and interdigitated back contact cells (Table 2c). These devices have been selected based on their outstanding conversion efficiency or special features. They represent the rapid progress of poly-Si passivating contacts in the laboratory and in mass production over the last decade.

On a cell, the poly-Si is typically applied on the rear surface to minimize parasitic absorption.[75] As such, cell structures with two-sided metallization commonly have boron or phosphorus diffused regions at the front surface and poly-Si at the rear. Both sides contacted cells can be further categorized into front or rear junction, in terms of minority-carrier collection, as shown in Table 2a. The highest reported efficiency for a both-sides-contacted solar cell at 26.0% (*device No. 2a-1*), is with a poly-Si rear junction, while the front junction configuration has the highest reported efficiency of 25.8% (*device No. 2a-2*).[28] Shifting the p-n junction to the back surface, by simply using a p-type wafer instead of an n-type, decouples the surface

TABLE 2a Small area silicon solar cells with poly-Si passivating contacts and both sides contacted

Device structure				V_{OC} (mV)	J_{SC} (mA/cm^2)	*FF* (%)	Efficiency (%)	Area (cm^2)	Wafer thickness (μm)	Certification	Year	Institution
No.	Front side	Substrate	Rear side									
2a-1	p^+ diff	p-type	SiO_x/**n^+ poly-Si**/Ag	732	42.1	84.3	26.0	4.0	245	CalLab/Fh-ISE	2021	Fh-ISE[64]
2a-2	p^+ diff	n-type	SiO_x/**n^+ poly-Si**/Ag	724	42.9	83.1	25.8	4.0	195	CalLab/Fh-ISE	2021	Fh-ISE[64]
2a-3	n^+ diff	p-type	SiO_x/**p^+ poly-Si**/Ag	701	41.1	79.9	23.0	4.0	200	*No*	2018	ANU[63]
2a-4	IO:Zr/**n^+ SiC_x**/SiO_x	p-type	SiO_x/**p^+ SiC_x**/IO:Zr	720	38.8	81.0	22.6	4.0	200	*No*	2018	EPFL[65]
2a-5	ITO/**a-Si (n)**/**a-Si(i)**	p-type	SiO_x/**p^+ SiC_x**/ITO	698	39.4	79.5	21.9	4.0	250	CalLab/Fh-ISE	2018	EPFL[73]

TABLE 2b Large area silicon solar cells with poly-Si passivating contacts and both sides contacted

Device structure				V_{OC} (mV)	J_{SC} (mA/cm^2)	*FF* (%)	Efficiency (%)	Area (cm^2)	Wafer thickness (μm)	Certification	Year	Institution
No.	Front side	Substrate	Rear side									
2b-1	*N/A*[a]	n-type	SiO_x/**n^+ poly-Si**	*N/A*	*N/A*	*N/A*	25.4	*N/A*	*N/A*	JET[b]	2021	Jinko[74]
2b-2	*N/A*	*N/A*	*N/A*	722	41.6	83.9	25.2	243.0	*N/A*	CalTeC/ISFH	2021	LONGi[54]
2b-3	p^+ diff	n-type	SiO_x/**n^+ poly-Si**	717	40.6	84.5	24.6	244.6	*N/A*	CalTeC/ISFH	2020	Trina[60]

[a]N/A: the data are not available.
[b]JET: Japan Electrical Safety and Environment Technology Laboratories.

passivation and lateral carrier transport roles of the front surface diffusion. This unlocks possibilities to further improve the V_{OC} and *FF* compared with the front p-n junction TOPCon cells. However, the collection efficiency is also reduced slightly, and the device becomes more sensitive to the bulk lifetime and the front surface passivation.[64] Partly due to the better performance of n^+ poly-Si, both sides contacted solar cells with p^+ poly-Si have received less attention, and the reported efficiency is lower in comparison, for example, *Device No. 2a-3* with efficiency of 23.0%. Although the application of p^+ poly-Si as full area rear junction is less impactful in comparison with n^+ poly-Si, the application of p^+ poly-Si together with n^+ poly-Si, such as in IBC devices as discussed below, can further improve the cell efficiency.

Doped polysilicon carbide (poly-SiC_x) has also been applied for p^+ and n^+ passivating contacts in solar cells, by adding methane to the silane during PECVD,[65] similar to the approach of using nc-SiC_x in SHJ technology. A small amount of carbon is introduced into the polysilicon layer to prevent blistering of the layer during the subsequent annealing process used to crystallize the layer. The addition of carbon also opens up the possibility of tuning the optical properties of the layer.[76] Doped p^+ and n^+ poly-SiC_X layers deposited on a front junction two-sided cell demonstrated excellent surface passivation with cell efficiency of 22.6% efficiency and V_{OC} of 720 mV (*device No. 2a-4*).[65] The cell suffered from a low J_{SC} due to parasitic absorption in the front n^+ SiC_X and TCO, but has only a single activation annealing step and lower thermal budget than the conventional approach. A similar approach with fast firing activation has also been reported, with an efficiency of 21.9% (*device No. 2a-5*).[73] It should be noted that the in-diffusion of dopants and the formation of a buried diffused region within the crystalline silicon wafer are avoided in the fired cells due to the limited thermal budget. This demonstrates that effective passivating contacts can be achieved without doping of the near-surface silicon region and highlights the role of the work function of the heavily doped polysilicon layer in establishing effective carrier population control.

Poly-Si has also been demonstrated in large-area cells in industry (Table 2b) with excellent results, highlighting the technology's compatibility with mass production. In addition to the longstanding

application of n^+ and p^+ poly-Si in IBC cells by SunPower with a reported efficiency of 25.2% (*device No. 2c-2*),[55] high efficiency cells featuring n^+ poly-Si have also been reported by various PV manufacturers, including Trina (*device No. 2b-3*)[60] and LONGI (*device No. 2b-2*).[77] The most recent efficiency benchmark for this category is from JinkoSolar with a conversion efficiency of 25.4% on a large area both sides contacted n-type cell (device No. *2b-1*).[74] In comparison to the front junction small-area cells, the lower efficiency of the large-area cells is mostly due to a lower J_{SC}. This is partly due to the larger shading fraction of screen-printed large area cells and increased free carrier absorption in the thicker poly-Si layer required for compatibility with screen printing. Parasitic absorption of up to 0.5 mA/cm^2 has been reported for a 145 nm thick poly-Si layer at the back with doping concentration of 1.9×10^{20} cm^{-3}.[75] It may be possible to decrease the thickness of the poly-Si layer with optimized screen printing paste or alternative metallization technology, such as copper electroplating.[78] Conversely, the V_{OC} and *FF* are comparable in the large-area cell, demonstrating the excellent surface passivation and contact resistivity of the poly-Si technology in mass production. With the application of poly-Si in industrial both sides contacted cells, the front surface recombination (usually including a p^+ boron diffusion) becomes the most significant loss. There have been attempts to reduce front contact recombination by applying the poly-Si locally under the metal contacts.[79] However, the gains in V_{OC} are currently offset by the losses in J_{SC}, from the wider poly-Si fingers required for alignment tolerance.

In IBC cells (Table 2c), either one or both junctions (i.e., the minority- and majority-carrier junctions/contacts) can be formed using poly-Si structures. The highest efficiency solar cell with poly-Si is the 4 cm^2 POLO-IBC cell with both junctions formed using poly-Si by ISFH at 26.1% (*device No. 2c-1*).[52] Compared with the front and back contact cells discussed above, the biggest gain for the IBC structure is in the *FF*. Intriguingly, the reported J_{SC} is slightly lower in comparison to the front junction TOPCon cell despite the thicker wafers used and the absence of front grid shading. This could be caused by multiple factors, such as a lower collection efficiency of back junction cells,[64] higher parasitic absorption in the thicker poly-Si,[75] or the lower reflectance of Al compared with Ag. A loss analysis performed on the POLO-IBC shows that a limiting factor is bulk recombination.[80] Even at such high efficiency, the surface recombination of the polysilicon passivating contact at the rear was not a significant limiting factor, which demonstrates the enormous potential of the technology.

Recently, poly-Si has also been applied as the front surface contacts on silicon bottom cells within perovskite-silicon monolithic tandem cells.[81] Similar to SHJ Si cells, the parasitic absorption in the poly-Si layers is less important because most of the short wavelength light is absorbed in the perovskite cell. Compared with SHJ-based Si bottom cells, poly-Si has better thermal stability and poses fewer restrictions in the selection and processing of the carrier selective contacts below the perovskite absorber,[82–84] Poly-Si has also been used to form the recombination junction in a tandem perovskite-silicon solar cell. A recombination junction with ITO and n-type poly-Si on a perovskite-silicon tandem solar cells has been demonstrated to allow a conversion efficiency of 21.3%.[84] The perovskite-silicon tandem solar cell with the p-type poly-Si deposited on top of the n-type poly-Si acting as the collecting junction in the Si bottom cell achieved an efficiency of 25.1%.[82]

4 | SILICON SOLAR CELLS WITH METAL-COMPOUND AND ORGANIC CONTACTS

There are many materials other than doped crystalline or amorphous silicon that, when deposited on a silicon wafer, can perform the function of selecting either electrons or holes. An initial motivation for exploring such materials was to overcome the optical limitations presented by doped a-Si:H (and also poly-Si); indeed, Battaglia et al., demonstrated an improved J_{SC} by replacing the a-Si(p):H layer at the front of a SHJ solar cell with MoO_x, whose wide optical bandgap and high work function (about 6 eV) made it very attractive for that purpose.[85] In the last 7 years, a multitude of other materials has been explored, fuelled by scientific curiosity and the attractiveness of their simplicity. Most of those materials, borrowed in some cases from thin film and organic solar cell technologies, are chemical compounds of various metals, including alkali/alkaline-earth metal compounds (AMC), transition metal oxides (TMO), and transition metal nitrides (TMN), with some effort dedicated to rare-earth compounds (REC), organic materials, and low work function (WF) metals like Mg, Ca, and Li. In principle, the fabrication of metal compound junctions on silicon can be very simple, involving just a wafer cleaning step followed by the

TABLE 2c Silicon solar cells with poly-Si passivating contacts and IBC structures

Device structure												
No.	Electron contact	Substrate	Hole contact	V_{OC} (mV)	J_{SC} (mA/cm^2)	*FF* (%)	Efficiency (%)	Area (cm^2)	Wafer thickness (μm)	Certification	Year	Institution
2c-1	SiO_x/**n$^+$ poly-Si**	p-type	SiO_x/**p$^+$ poly-Si**	727	42.6	84.3	26.1	4.0	300	CalTeC/ ISFH	2018	ISFH[52]
2c-2	SiO_x/**n$^+$ poly-Si**	n-type	SiO_x/**p$^+$ poly-Si**	737	41.3	82.7	25.2	153.0	130	CalLab/Fh-ISE	2016	SunPower[55]
2c-3	SiO_x/**n$^+$ poly-Si**	n-type	*N/A*	716	42.3	82.8	25.0	243.0	*N/A*	JET	2019	Trina[56]

deposition of the material in question, without the need for dopant sources or high temperature doping processes. In practice, most of these materials lack the ability to passivate surface defects and an extra step is required to deposit a passivating interlayer. Thin metal compound films can be deposited by many different methods, for example, thermal evaporation, sputtering, atomic layer deposition (ALD), and through solution processing, with methods involving H-rich precursors (such as organometallic vapours for ALD) frequently preferred to achieve chemical passivation. Thermal evaporation is one of the most used methods, as it simply involves sublimating the material from a stoichiometric powder source using a facility, the thermal evaporator, that most laboratories have access to. The process does not require a high level of optimization, besides aiming for very low deposition pressures, due to many powder sources being highly hygroscopic. In some cases, decomposition of the powder happens during sublimation and the chemical composition of the films differs from that of the source (e.g., LiN_x yielding metallic Li),[86] which can be desirable (e.g., oxygen-deficient MoO_x). Metal compound solutions can also be easily prepared by dissolving the powder in a suitable solvent and then spin-coating on the silicon wafer.

Within each of the chemical families mentioned above, we find materials with a wide range of work function values, and hence some of them are appropriate to select electrons (typically when they have a low WF), whereas others are suitable to select holes (typically when their WF is high). Because of that, we classify the solar cells in this section according to the functionality of the contact, either as electron-selective (Table 3a) or as hole-selective (Table 3b), with a third group dedicated to devices where both selective contacts are made with metal compounds (Table 3c). It is important to keep in mind that the final performance of a given solar cell is determined by many factors, and it may not reflect faithfully the true potential of a given contact material or structure. Most of the devices in this section have just one of the two carrier-selective junctions implemented with a metal compound or organic material, and hence their performance may be affected by the other junction, or by the optical coatings used, the metallization technique, the quality of the silicon wafer, and so forth. It is also important to note that the amount of effort dedicated to developing solar cells with metal compound and organic junctions has been quite limited, which explains to some extent the relatively modest efficiencies achieved so far for many of them. To avoid an excessively large set of data, while giving a sufficiently broad overview of the many materials that have been explored, we only present here devices with an efficiency higher than 19%, with the exception of one industrially sized solar cell.

Although carrier selection is relatively easy with materials having an extreme WF, achieving a low recombination at the interface between them and the silicon wafer is more problematic. There are two approaches to circumvent this. The first is to add a dedicated passivation interlayer to a full-area contact, which also helps to reduce the effect of Fermi energy pinning, ubiquitous for directly metallized silicon (*devices No. 3a-1* to *3a-7*, *3b-1*, *3b-2*, *3c-1*, and *3c-2)*. The most commonly used interlayers are intrinsic a-Si(i):H, SiO_x and TiO_x, the first providing the best passivation, as evidenced by the high V_{OC} achieved by *device No. 3b-1* (734 mV[104]). The second approach, akin to the industry standard PERC design, is to restrict the contact area to a small fraction of the surface of the silicon wafer, while applying a non-conductive passivation layer to the rest. This was first demonstrated for n-type Si in 2016 with an electron-selective LiF_x/Al contact applied to just 1% of the rear surface, achieving a 20.6% conversion efficiency (*device No. 3a-19*). Combining both approaches, that is, adding a passivating interlayer to a localized contact, permits to increase V_{OC} and conversion efficiency, as shown by *device No. 3a-17* (TiO_x/Ca/Al partial area contact[103]) and *device No. 3a-16* (TiO_x/LiF_x/Al partial area contact[100]).

The results in the three tables indicate that the presence of a dedicated passivating interlayer is necessary to achieve a truly high conversion efficiency. Both the partial-area approach with a TiO_x interlayer, and the full-area approach with an a-Si(i):H interlayer, have produced efficiencies over 23%. The 23.1% efficiency of *device No. 3a-16*, which has a TiO_x/LiF_x/Al partial rear contact, is the highest of those having a metal-compound electron-selective contact. The highest efficiency for devices with a hole-selective contact is 23.5%, corresponding to a modified SHJ solar cell having a MoO_x hole-selective junction at the front side (*device No. 3b-1*). In a controlled experiment (the experiment included two solar cells that were identical to each other apart from their hole contacts, one used a-Si(p):H and another one used MoO_x) the use of MoO_x instead of a-Si(p):H led to a 1.3 mA/cm^2 higher J_{SC}.[104] Nevertheless, the advantage of a wide optical bandgap, also presented by other materials in this section, is curtailed by the need to transport electric current vertically, which places limitations on how thick the layer can be and makes it ineligible as an ARC (anti-reflection coating). This is well illustrated by MgF_x, frequently used in double ARCs for high-performance solar cell prototypes,[64] but needs to be extremely thin (2 nm in *device No. 3a-5*) when used for carrier selection.[91] Like MgF_x, most of the other metal compounds in this section are poor conductors, and their thickness needs to be restricted to a few nm (just 1 nm in some cases) to achieve a sufficiently low contact resistance. There are a few exceptions, like TiN_x and PEDOT:PSS, which are good conductors, although they both incur a large amount of parasitic absorption. When placed at the front, these thin metal-compound layers and organic materials need the assistance of a transparent conductive oxide to transport current laterally (*devices No.3b-1*, *No. 3b-3*, *No. 3c-1*, and *No. 3c-2*), which in turn poses a limit on the transparency of the whole selective contact structure, as discussed in the context of SHJ devices.

It is noticeable, by looking at the tables, that there is a much greater diversity of electron-selective materials than hole-selective ones. Among the latter, only transition metal oxides and organic materials have been successfully demonstrated, whereas among the electron-selective contacts we also find transition metal nitrides, alkali/alkaline-earth compounds (and metals) and rare earth compounds. There is one device in Table 3a with an organic electron-selective contact reaching an efficiency of above 19% (*device No. 3a-7*), although more organic-based electron-selective contacts have been demonstrated successfully, for example, dipole materials.[115] On the other hand, hole-selective contacts are the only ones

TABLE 3a Both sides contacted silicon solar cells with metal compounds/organics as electron contacts

Device structure					Extra passivation layer	Material category	Work function (eV)	V_{OC} (mV)	J_{SC} (mA/cm^2)	*FF* (%)	Efficiency (%)	Area (cm^2)	Year	Institution
No.	Front side	Substrate	Rear side	Geometry										
3a-1	p$^+$ diff.	n-type	a-Si(i):H/**CsF** (2 nm) /Al	Full area	a-Si(i):H (6 nm)	AMC	3.0	688	40.1	78.9	21.8	4.0	2020	SJTU & ANU[87]
3a-2	p$^+$ diff.	n-type	a-Si(i):H/ **CaAcac**[a] (1 nm) /Al	Full area	a-Si (i):H (6.5 nm)	AMC	2.5	687	39.5	79.5	21.6	4.0	2020	SYSU & ANU[88]
3a-3	p$^+$ diff.	n-type	SiOx/**TiO$_x$** (3.5 nm) /Al	Full area	SiO$_x$ (1.7 nm)	TMO	*N/A*	676	39.6	80.7	21.6	4.0	2016	ANU[89]
3a-4	p$^+$ diff.	n-type	**TiO$_x$** (4 nm) /**LiF** (1 nm) /Al	Full area	TiO$_x$ (5 nm)	TMO-AMC	*N/A*	660	40.8	79.2	21.3	4.0	2019	ANU[90]
3a-5	p$^+$ diff.	n-type	a-Si(i):H/**MgF$_x$** (2 nm) /Al	Full area	a-Si(i):H (6.5 nm)	AMC	3.0	687	37.8	77.3	20.1	4.0	2016	ANU[91]
3a-6	p$^+$ diff.	n-type	SiOx/**TiN$_x$** (300 nm) /Al	Full area	SiO$_x$ (1.2 nm)	TMN	4.3	644	37.9	81.9	20	4.0	2019	KAUST & ANU[92]
3a-7	ITO/a-Si (p)/a-Si (i)	n-type	a-Si(i)/**b-PEI**[b] (3 nm) /Al	Full area	a-Si(i):H (6 nm)	Organic	2.9	720	37.0	72.9	19.4	4.0	2020	KAUST&UCB[93]
3a-8	p$^+$ diff.	n-type	**EuF$_x$** (4 nm) / Al/Ag	Full area	*N/A*	REC	3.7	663	40.4	80.5	21.6	4.0	2021	SYSU[94]
3a-9	p$^+$ diff.	n-type	**TaN$_x$** (2.5 nm) /Al	Full area	*N/A*	TMN	4.3	632	38.8	81.8	20.1	4.0	2018	KAUST & ANU[95]
3a-10	p$^+$ diff.	n-type	**MgO$_x$** (1 nm) /Al	Full area	*N/A*	AMC	4.1	629	39.5	80.6	20.0	4.0	2016	ANU[96]
3a-11	p$^+$ diff.	n-type	**TiO$_x$** (4.5 nm) /Al	Full area	*N/A*	TMO	*N/A*	638	39.2	79.1	19.8	4.0	2016	ANU[89]
3a-12	p$^+$ diff.	n-type	**CsF** (2 nm) /Al	Full area	*N/A*	AMC	2.96	621	38.9	80.3	19.4	4.0	2020	SJTU[97]
3a-13	p$^+$ diff.	n-type	**K$_2$C$_x$O$_y$** (1 nm) /Al	Full area	*N/A*	AMC	*N/A*	624	38.9	80.0	19.4	4.0	2018	ANU[98]
3a-14	p$^+$ diff.	n-type	**Li**/Al	Full area	*N/A*	AMC	2.9	619	37.9	81.1	19.0	4.0	2021	KAUST[86]
3a-15	p$^+$ diff.	n-type	a-Si(i):H/**Mg** (10 nm) /Al	Full area	a-Si(i):H (6 nm)	AMC	3.7	637	38.0	78.4	19.0	4.0	2016	ANU[99]
3a-16	p$^+$ diff.	n-type	**TiO$_x$/LiF** (1 nm) /Al	**Partial area ($f_c \sim$ 1%)**[c]	TiO$_x$ (1.5 nm)	TMO-AMC	3.8 TiO$_x$	695	41.5	80.0	**23.1**	4.0	2019	UCB & ANU[100]
3a-17	p$^+$ diff.	n-type	**TiO$_x$/Ca** (30 nm) /Al	**Partial area ($f_c \sim$ 6.25%)**	TiO$_x$ (3.5 nm)	TMO-AMC	*N/A*	681	39.6	80.9	21.8	4.0	2017	ANU[101]

TABLE 3a (Continued)

Device structure					Extra passivation layer	Material category	Work function (eV)	V_{OC} (mV)	J_{SC} (mA/cm^2)	*FF* (%)	Efficiency (%)	Area (cm^2)	Year	Institution
No.	**Front side**	**Substrate**	**Rear side**	**Geometry**										
3a-18	p^+ diff.	n-type	**CeF_3** (1.5 nm) /Al	**Partial area**[d]	*N/A*	REC	3.16	*646*	41.6	79.1	21.3	4.0	2021	SYSU[97]
3a-19	p^+ diff.	n-type	**LiF_x** (1 nm)/Al	**Partial area ($f_c \sim 1\%$)**	*N/A*	AMC	28	*676*	38.9	78.3	20.6	4.0	2016	ANU & UCB[102]
3a-20	p^+ diff.	n-type	**Ca** (30 nm) /Al	**Partial area ($f_c \sim 1.26\%$)**	*N/A*	AMC	2.9 (Ca)	*652*	39.6	78.6	20.3	4.0	2016	ANU[103]

[a]CaAcacs: calcium acetylacetones.
[b]b-PEI: branched polyethylenimine.
[c]f_c: contact fraction.
[d]25 μm diameter open area.

demonstrated so far on large area solar cells. In the two examples given in Table 3b, a 20.2% efficient cell with a PEDOT:PSS contact (*device No. 3b-5*) and a 17.7% cell with a MoO_x contact (*device No. 3b-6*), which intends to replace the aluminum partial rear contact typical of industrial p-type cells. The organic or metal oxide compounds are applied to the whole rear surface, which can be advantageous in terms of one-directional current flow (e.g., a vertical current flow), thus permitting to use a wider range of wafer resistivities, and process simplicity.[8]

An interesting observation is that all the electron-selective contacts/junctions in Table 3a have been placed at the back of n-type wafers, whereas most of the hole-selective contacts in Table 3b were formed at the back of p-type wafers. That is, most of the metal compound and organic materials have been demonstrated at the solar cell level as unipolar junctions or, in other words, as selective contacts for the carriers that are the majority within the silicon wafer. Given that the silicon wafer itself provides some level of asymmetric conductivity, it is logical to expect that a certain material will function as a majority-carrier junction more easily than as a minority-carrier one. Only in a few of the devices presented in Table 3b is the minority-carrier junction implemented with a metal compound. Their ability to do so has been attributed to either a very high work function (MoO_x and WO_x) or a high negative charge (oxygen-deficient TiO_x), so that an inversion layer forms in the silicon wafer, that is, an induced pn junction. Although not shown in these tables, it is worth mentioning that working devices with LiF_x/Al as a bipolar junction (that is, on a p-type wafer) have also been demonstrated.[116]

The case of TiO_x deserves special mention because it can have ambipolar behavior, depending on the deposition method, capping layer and post-deposition treatment.[106] As shown in Table 3a, TiO_x has been utilized mostly on n-type solar cells as part of the electron-selective contact, due to the expected good alignment between its conduction band and that of silicon. In some instances,[90,100,103] TiO_x is assisted by low work function materials, like LiF_x/Al and Ca to achieve Ohmic current transport with a low contact resistance, in which case the main carrier-selective material is LiF_x/Al or Ca, whereas TiO_x's principal role is as a passivating interlayer. Recently, it has been demonstrated[106] that TiO_x can be modified so that it functions as a hole-selective material, as shown in *device No. 3b-26*. Such selectivity has been attributed to a high negative charge together with a high work function ITO capping layer, creating an inversion layer within the n-type Si wafer.[106] Although *FF* and V_{OC} are significantly lower than those of a control cell with an ITO/a-Si(p):H/a-Si(i):H front junction, a 1.5 mA/cm^2 improvement in J_{SC}, resulting from an improved transparency, led to a 21.1% conversion efficiency.[106]

Finally, devices where both carrier-selective contacts are made with metal-compounds are presented in Table 3c. The first high efficiency "dopant-free asymmetric heterojunction" solar cell was reported in 2016 (*device No. 3c-4*) and achieved a 19.7% conversion efficiency.[116] Adding a second TiO_x passivating interlayer to the LiF_x/Al electron-selective contact, while maintaining a two-sided metallization, increased the efficiency to 20.7% (*device No. 3c-2*).[113] Lastly, a

TABLE 3b Silicon solar cells with metal compounds/organics as hole contacts

Device structure					Extra passivation layer	Material category	Work function (eV)	V_{OC} (mV)	J_{SC} (mA/cm^2)	*FF* (%)	Efficiency (%)	Area (cm^2)	Year	Institution
No.	Front side	Substrate	Rear side	Geometry										
3b-1	Ag/ITO/**MoO_x** (4 nm)/a-Si (i)	n-type	a-Si(i):H/a-Si (n):H/ITO	Full area	a-Si(i):H (8 nm)	TMO	6.0	734	39.2	81.8	**23.5**[a]	4.0	2020	EPFL[104]
3b-2	ITO/a-Si (n) /a-Si(i)	n-type	a-Si(i):H/**V_2O_x**(4.5 nm) /ITO/Ag	Full area	a-Si(i):H (5 nm)	TMO	6.0	721	38.3	78.2	21.6	4.0	2020	KAUST[105]
3b-3	Ag/ITO/**TiO_x** (5 nm)	n-type	a-Si(i):H/a-Si(n):H/ITO	Full area	*N/A*	TMO	*N/A*	677	40.5	76.8	21.1	4.0	2020	AIST & Fraunhofer ISE[106]
3b-4	n^+ diff.	p-type	**PEDOT:PSS** (184 nm) /Ag	Full area	*N/A*	Organic	*N/A*	660	38.5	80.0	20.4	4.0	2019	ISFH[107]
3b-5	n^+ diff.	p-type	**PEDOT:PSS** (170 nm) /Ag	Full area	*N/A*	Organic	*N/A*	656	38.7	79.5	20.2	**243.4**	2018	ISFH[108]
3b-6	n^+ diff.	p-type	**MoO_x** (20 nm) /Ag	Full area	*N/A*	TMO	*N/A*	626	36.8	76.6	17.7	**243.4**	2020	METU[58]
3b-7	n^+ diff.	p-type	**MoO_x** (15 nm) /Ag	**Partial area ($f_c \sim$ 5%)**	*N/A*	TMO	*N/A*	658	39.8	77.8	20.4	4.0	2015	ANU[109]
3b-8	n^+ diff.	p-type	**CrO_x** (2 nm) / **Ag** (30 nm)/**CrO_x** (2 nm)/ Ag	**Partial area**[b]	*N/A*	TMO	4.8	638	39.8	80.1	20.3	4.0	2018	SYSU[110]
3b-9	Al_2O_3/a-SiC (i)/	n-type	n^+ diff. / Al (*Electron*) **V_2O_x** (40 nm)/Ni/Al (*Hole*)	**IBC**	*N/A*	TMO	*N/A*	656	40.7	74.0	19.7	9.0	2013	UPC[111]

[a]Certified by CalTeC/ISFH.
[b]With a pitch length of 920 μm).

TABLE 3c Both sides contacted and IBC silicon solar cells with metal compounds as both electron and hole contacts

Device structure											
No.	Electron contact	Substrate	Hole contacts	Geometry	V_{OC} (mV)	J_{SC} (mA/cm^2)	*FF* (%)	Efficiency (%)	Area (cm^2)	Year	Institution
3c-1	a-Si(i):H/**MgF_x**/Al/Ag	n-type	a-Si(i):H/**MoO_x**/Ag	**IBC**	709	41.5	75.6	22.2	4.5	2019	SYSU & EPFL[112]
3c-2	Ag/ITO/**MoO_x**/a-Si(i):H	n-type	a-Si(i):H/**TiO_x**/**LiF** (0.6 nm)/Al	Full area	706	38.4	76.2	20.7	4.0	2018	UCB, ANU, & EPFL[113]
3c-3	a-Si(i):H/**TiO_x**/**Mg**/Al/Ag	n-type	a-Si(i):H/**MoO_x**/Ag/Al	**IBC**	694	38.6	75.3	20.2	1.0	2019	UCAS[114]
3c-4	Ag/ITO/**MoO_x**/a-Si(i):H	n-type	a-Si(i):H/**LiF**/Al	Full area	716	37.0	73.2	19.4	4.0	2016	UCB, ANU & EPFL[67]

22.2% efficiency (*device No. 3c-1*) and a 20.24% efficiency (*device No. 3c-3*) have been achieved with an IBC (Interdigitated back contact) device structure and either a MgF_x or a TiO_x/Mg electron-selective contact, respectively,[114,117] All four solar cells in the Table 3c are made on n-type silicon, use a-Si(i):H as passivating interlayer, and rely on MoO_x to form the hole-selective (i.e., minority-carrier) junction. Their *FF* values are relatively low, indicating that more work is needed to improve contact resistance, overall device design and fabrication. It should also be noted that initial attempts to make bifacial cells using a set of metal compound layers have also been made, most notably Lin et al.[118] However, the development of a transparent/stable electron contact remains an ongoing research challenge hindering this architecture.

The metal compound and organic materials presented in this section offer great versatility to the solar cell designer and allow for simple fabrication schemes. However, there are some shortcomings that need to be tackled, the most important being: the passivation quality is not as high as that of doped-silicon passivating contact approaches, they show poor-to-moderate thermal stability, and some of the deposition tools and processes are not common in current industrial production of c-Si solar cells. The degree to which these shortcomings are present depends on each material. For instance, organic-based films normally suffer from much more severe thermal instability than metal compound structures, some of which have been shown to be stable up to 400°C,[88,97] which is above the thermal budget of the classical SHJ process. Note also how some material families can provide a modest level of passivation on c-Si, even when deposited using hydrogen-free processes (e.g., metal oxides), while for others this is almost impossible (e.g., metal halides). Another important practical limitation is the strict thickness control required for most of the films, which is more difficult to achieve in a high-throughput production line. The main takeaway is that finding a material that can meet the aforementioned requirements and compete against doped silicon remains an ongoing research challenge.

5 | CONCLUSION

The breadth of architectural variation and demonstrated efficiencies of cells listed in Tables 1, 2, and 3 reflect the growing opportunities offered by passivating contacts in silicon solar cells. These opportunities are being explored by many of the larger PV companies who are responsible for several of the entries in these tables around and above 25%, with others not far behind. As more companies are able to achieve significant efficiency margins over the conventional PERC technology by using passivated contacts, the market share of passivated contact technologies will grow, with some sources predicting above 50% of the total market by the year 2031.[37]

Also reflected in Tables 1, 2, and 3 is an opportunity to mix and match contacting approaches, creating what may be described as "hybrid" cells. For example, the most common implementation of poly-Si contact technology utilizes a boron diffusion at the front of an n-type wafer, and the most successful example of metal compounds at 23.5% uses MoO_x in the place of a-Si(p):H in the conventional SHJ cell. This suggests the possibility of a more architecturally diverse future market and highlights opportunities for new combinations where compatibilities permit, for example, metal compounds and poly-Si contacts.

Finally, as highlighted in the above sections, passivating contacts are proving to be an enabling technology for efficiencies beyond 26% via concepts such as IBC cells and tandem devices. The passivating contact interfaces permit a larger percentage of the surface area to be contacted without incurring recombination, which may simplify the IBC fabrication procedure, as evidenced by Kaneka's IBC demonstration at 26.7%. The same strengths of passivated contacts are being utilized in tandem cells. For example, the majority of groups working on monolithic perovskite/silicon tandem cells, now producing cells with efficiencies up to and above 29%, utilize full area SHJ contacts to interface with the top perovskite cell (noting that the cell structure

of the current record perovskite/silicon tandem cell, produced by Oxford PV, has not been made publicly available).[43]

Regardless of the specific implementation, it is clear that passivating the contacts of silicon solar cells is an essential step in advancing the silicon PV industry beyond the 24–25% mark. At present, cells utilizing SHJ and poly-Si-based passivated contacts have already been demonstrated above 26%, trailed by cells employing metal compound passivated contacts, where the efficiency benchmark is 23%. Based on this exciting trajectory, it is safe to say the coming years will see the development of an even broader library of passivated contact approaches to fuel a post-25% terrestrial PV industry.

ACKNOWLEDGMENTS

This work has been supported by the Australian Renewable Energy Agency (ARENA) via the Australian Centre for Advanced Photovoltaics (ACAP). J.B., J.S., and T.K. acknowledge support from ACAP Fellowships.

ORCID

Teng Choon Kho https://orcid.org/0000-0002-8578-323X
James Bullock https://orcid.org/0000-0001-7903-9642

REFERENCES

1. Kruse CN. Characterization and loss analyses of passivated emitter and rear cells, doctoralThesis, Hannover: Institutionelles Repositorium der Leibniz Universität Hannover. 2020. 10.15488/9941
2. Green MA, Blakers AW, Willison ZR, et al. The MINP solar cell—A new high voltage, high efficiency silicon solar cell. 1981:1405-1408. Accessed: Sep. 25, 2021. [Online]. Available: https://ui.adsabs.harvard.edu/abs/1981pvsp.conf.1405G
3. Zielke D, Petermann JH, Werner F, Veith B, Brendel R, Schmidt J. Contact passivation in silicon solar cells using atomic-layer-deposited aluminum oxide layers. *Phys Status Solidi RRL – Rapid Res Lett*. 2011;5(8):298-300. doi:10.1002/pssr.201105285
4. Bullock J, Yan D, Wan Y, et al. Amorphous silicon passivated contacts for diffused junction silicon solar cells. *J Appl Phys*. 2014;115(16):163703. doi:10.1063/1.4872262
5. Glunz SW, Steinhauser B, Polzin JI, et al. Silicon-based passivating contacts: The TOPCon route. *Prog Photovolt Res Appl*. 2021:1-19. doi:10.1002/pip.3522
6. Allen TG, Bullock J, Yang X, Javey A, De Wolf S. Passivating contacts for crystalline silicon solar cells. *Nat Energy*. 2019;4(11):914-928. doi:10.1038/s41560-019-0463-6
7. Melskens J, van de Loo BW, Macco B, Black LE, Smit S, Kessels WM. Passivating contacts for crystalline silicon solar cells: from concepts and materials to prospects. *IEEE J Photovolt*. 2018;8(2):373-388. doi:10.1109/JPHOTOV.2018.2797106
8. Glunz S, Feldmann F, Richter A, et al. The irresistible charm of a simple current flow pattern—25% with a solar cell featuring a full-area back contact. 2015. 10.4229/EUPVSEC20152015-2BP.1.1
9. Sark WV, Korte L, Roca F (Eds). *Physics and Technology of Amorphous-Crystalline Heterostructure Silicon Solar Cells*. Springer; 2012. doi:10.1007/978-3-642-22275-7
10. Cuevas A, Wan Y, Yan D, et al. Carrier population control and surface passivation in solar cells. *Sol Energy Mater sol Cells*. 2018;184:38-47. doi:10.1016/j.solmat.2018.04.026
11. Würfel U, Cuevas A, Würfel P. Charge carrier separation in solar cells. *IEEE J Photovolt*. 2015;5(1):461-469. doi:10.1109/JPHOTOV.2014.2363550
12. Zhao Y, Mazzarella L, Procel P, et al. Ultra-thin electron collectors based on nc-Si:H for high-efficiency silicon heterojunction solar cells. *Prog Photovolt Res Appl*. 2021:1-4. doi:10.1002/pip.3502
13. Singh S, Choulat P, Govaerts J, et al. Large area co-plated bifacial n-PERT cells with polysilicon passivating contacts on both sides. *Prog Photovolt Res Appl*. 2022:1-11. doi:10.1002/pip.3548
14. Nandakumar N, Rodriguez JW, Padhamnath P, Nampalli N, Aberle AG, Duttagupta S. Large-area monoPoly solar cells on 110 μm thin c–Si wafers with a rear n+poly-Si/SiOx stack deposited by inline plasma-enhanced chemical vapour deposition. *Prog Photovolt Res Appl*. 2022:1-9. doi:10.1002/pip.3555
15. Michel JI, Dréon J, Boccard M, Bullock J, Macco B. Carrier-selective contacts using metal compounds for crystalline silicon solar cells. *Prog Photovolt Res Appl*. 2022:1-34. doi:10.1002/pip.3552
16. Fuhs W, Niemann K, Stuke J. Heterojunctions of Amorphous Silicon and Silicon Single Crystals, in TETRAHEDRALLY BONDED AMORPHOUS SEMICONDUCTORS: International Conference, Yorktown Heights, New York (USA); 1974:345-350. doi:10.1063/1.2945985
17. Pankove JI, Tarng ML. Amorphous silicon as a passivant for crystalline silicon. *Appl Phys Lett*. 1979;34(2):156-157. doi:10.1063/1.90711
18. Taguchi M, Tanaka M, Matsuyama T, et al. Tech. Digest 5th International Photovoltaic Science and Engineering Conference, Kyoto, Japan; 1990.
19. Tanaka M, Taguchi M, Matsuyama T, et al. Development of new a-Si/c-Si heterojunction solar cells: ACJ-HIT (artificially constructed junction-heterojunction with intrinsic thin-layer). *Jpn J Appl Phys*. 1992;31(Part 1, 11):3518-3522. doi:10.1143/JJAP.31.3518
20. Taguchi M, Yano A, Tohoda S, et al. 24.7% Record efficiency HIT solar cell on thin silicon wafer. *IEEE J Photovolt*. 2014;4(1):96-99. doi:10.1109/JPHOTOV.2013.2282737
21. Seif JP, Krishnamani G, Demaurex B, Ballif C, De Wolf S. Amorphous/crystalline silicon interface passivation: ambient-temperature dependence and implications for solar cell performance. *IEEE J Photovolt*. 2015;5(3):718-724. doi:10.1109/JPHOTOV.2015.2397602
22. Le AH, Basnet R, Yan D, et al. Temperature-dependent performance of silicon solar cells with polysilicon passivating contacts. *Sol Energy Mater sol Cells*. 2021;225:111020. doi:10.1016/j.solmat.2021.111020
23. Holman ZC, Descoeudres A, Barraud L, et al. Current losses at the front of silicon heterojunction solar cells. *IEEE J Photovolt*. 2012;2(1):7-15. doi:10.1109/JPHOTOV.2011.2174967
24. Cruz A, Wang EC, Morales-Vilches AB, et al. Effect of front TCO on the performance of rear-junction silicon heterojunction solar cells: insights from simulations and experiments. *Sol Energy Mater sol Cells*. 2019;195:339-345. doi:10.1016/j.solmat.2019.01.047
25. Descoeudres A, Horzel J, Paviet-Salomon B, et al. The versatility of passivating carrier-selective silicon thin films for diverse high-efficiency screen-printed heterojunction-based solar cells. *Prog Photovolt Res Appl*. 2020;28(6):569-577. doi:10.1002/pip.3227
26. Köhler M, Pomaska M, Procel P, et al. A silicon carbide-based highly transparent passivating contact for crystalline silicon solar cells approaching efficiencies of 24%. *Nat Energy*. 2021;6(5):529-537. doi:10.1038/s41560-021-00806-9
27. Bhambhani A. 26.30% Efficiency For LONGi's HJT Solar Cell | Taiyang News. http://taiyangnews.info/technology/26-30-efficiency-for-longis-hjt-solar-cell/ (accessed Dec. 20, 2021).
28. Suzhou Maxwell/SunDrive Solar, 25.54%! New world record for full-size batteries! | PV-Tech Daily Photovoltaic News. http://www.pv-tech.cn/news/25.54_New_world_record_for_full-size_battery
29. Huasun. 25.26%!Beyond ourselves again, ANHUI HUASUN refreshed the highest efficiency of silicon heterojunction SOLAR cells. https://huasun.net/2021/08/huasun25_26-new-world-record-of-hjt-solar-cell-efficiency/

30. Ru X, Qu M, Wang J, et al. 25.11% efficiency silicon heterojunction solar cell with low deposition rate Intrinsic amorphous silicon buffer layers. *Sol Energy Mater sol Cells*. 2020;215:110643. doi:10.1016/j.solmat.2020.110643
31. Yamamoto K, Yoshikawa K, Uzu H, Adachi D. High-efficiency heterojunction crystalline Si solar cells. *Jpn J Appl Phys*. 2018;57(8):08RB20. doi:10.7567/JJAP.57.08RB20
32. Yoshikawa K, Yoshida W, Irie T, et al. Exceeding conversion efficiency of 26% by heterojunction interdigitated back contact solar cell with thin film Si technology. *Sol Energy Mater sol Cells*. 2017;173(April):37-42. doi:10.1016/j.solmat.2017.06.024
33. Masuko K, Shigematsu M, Hashiguchi T, et al. Achievement of more than 25% conversion efficiency with crystalline silicon heterojunction solar cell. *IEEE J Photovolt*. 2014;4(6):1433-1435. doi:10.1109/JPHOTOV.2014.2352151
34. Tomasi A, Paviet-Salomon B, Jeangros Q, et al. Simple processing of back-contacted silicon heterojunction solar cells using selective-area crystalline growth. *Nat Energy*. 2017;2(5):17062. doi:10.1038/nenergy.2017.62
35. Wright M, Stefani BV, Soeriyadi A, et al. Progress with defect engineering in silicon heterojunction solar cells. *Phys Status Solidi Rapid Res Lett*. 2021;15(9):2100170. doi:10.1002/pssr.202100170
36. Wang Y. Mono wafer updates as substrate for High efficiency solar cell, presented at the 3rd International Workshop on Silicon Heterojunction Solar Cells, Shanghai, Japan, Oct. 20, 2020.
37. VDMA. International Technology Roadmap for Photovoltaic (ITRPV), 2021. [Online]. Available: https://itrpv.vdma.org/documents/27094228/29066965/20210ITRPV/08ccda3a-585e-6a58-6afa-6c20e436cf41
38. Mazzarella L, Kirner S, Stannowski B, Korte L, Rech B, Schlatmann R. p-type microcrystalline silicon oxide emitter for silicon heterojunction solar cells allowing current densities above 40 mA/cm ^{2}. *Appl Phys Lett*. 2015;106(2):023902. doi:10.1063/1.4905906
39. Zhang Y, Yu C, Yang M, et al. Optimization of the window layer in large area silicon heterojunction solar cells. *RSC Adv*. 2017;7(15):9258-9263. doi:10.1039/C6RA26342A
40. Boccard M, Holman ZC. Amorphous silicon carbide passivating layers for crystalline-silicon-based heterojunction solar cells. *J Appl Phys*. 2015;118(6):065704. doi:10.1063/1.4928203
41. Zhang D, Deligiannis D, Papakonstantinou G, van Swaaij RA, Zeman M. Optical enhancement of silicon heterojunction solar cells with hydrogenated amorphous silicon carbide emitter. *IEEE J Photovolt*. 2014;4(6):1326-1330. doi:10.1109/JPHOTOV.2014.2344768
42. Pingel S, Erath D, Wenzel T, et al. Low-temperature Ag-Paste Screening for Silicon Heterojunction Solar Cells and Modules, 37th Eur Photovolt sol Energy Conf Exhib, 508-511, 2020. doi:10.4229/EUPVSEC20202020-2DV.3.17
43. Oxford PV celebrates 29.5% conversion rate with perovskite solar cell, Solar Power Portal. https://www.solarpowerportal.co.uk/news/oxford_pv_celebrates_29.5_conversion_rate_with_perovskite_solar_cell (accessed Sep. 27, 2021).
44. HZB hits 29.15% efficiency with perovskite/silicon tandem cell. https://renewablesnow.com/news/hzb-hits-2915-efficiency-with-perovskitesilicon-tandem-cell-685469/ (accessed Sep. 27, 2021).
45. Gan JY, Swanson RM. Polysilicon emitters for silicon concentrator solar cells. *IEEE Conf Photovolt Special*. 1990;1:245-250. doi:10.1109/PVSC.1990.111625
46. Kwark YH, Swanson RM. N-type SIPOS and poly-silicon emitters. *Solid-State Electron*. 1987;30(11):1121-1125. doi:10.1016/0038-1101(87)90076-1
47. Kwark YH, Sinton R, Swanson RM. SIPOS Heterojunction contacts to silicon. In: *1984 International Electron Devices Meeting*. IEEE; 1984:742-745. doi:10.1109/IEDM.1984.190832
48. Yablonovitch E, Gmitter T, Swanson RM, Kwark YH. A 720 mV open circuit voltage SiOx:c-Si:SiOx double heterostructure solar cell. *Appl Phys Lett*. 1985;47(11):1211-1213. doi:10.1063/1.96331
49. Lindholm FA, Neugroschel A, Arienzo M, Iles PA. Heavily doped polysilicon-contact solar cells. *IEEE Electron Device Lett*. 1985;6(7):363-365. doi:10.1109/EDL.1985.26155
50. Green MA, Blakers AW. Advantages of metal-insulator-semiconductor structures for silicon solar cells. *Sol Cells*. 1983;8(1):3-16. doi:10.1016/0379-6787(83)90036-4
51. Feldmann F, Bivour M, Reichel C, Hermle M, Glunz SW. Passivated rear contacts for high-efficiency n-type Si solar cells providing high interface passivation quality and excellent transport characteristics. *Sol Energy Mater sol Cells*. 2014;120:270-274. doi:10.1016/j.solmat.2013.09.017
52. Haase F, Hollemann C, Schäfer S, et al. Laser contact openings for local poly-Si-metal contacts enabling 26.1%-efficient POLO-IBC solar cells. *Sol Energy Mater sol Cells*. 2018;186:184-193. doi:10.1016/j.solmat.2018.06.020
53. Steinhauser B, Polzin JI, Feldmann F, Hermle M, Glunz SW. Excellent surface passivation quality on crystalline silicon using industrial-scale direct-plasma TOPCon deposition technology. *Sol RRL*. 2018;2(7):1800068. doi:10.1002/solr.201800068
54. LONGi Solar. LONGi breaks three more world records for solar cell efficiency. http://www.longi-solar.com.au/home/events/press_detail/id/335_LONGi_breaks_three_more_world_records_for_solar_cell_efficiency_.html (accessed Sep. 06, 2021).
55. Smith DD, Reich G, Baldrias M, Reich M, Boitnott N, Bunea G. Silicon solar cells with total area efficiency above 25%. In: *2016 IEEE 43rd Photovoltaic Specialists Conference (PVSC)*. IEEE; 2016:3351-3355. doi:10.1109/PVSC.2016.7750287
56. Xu G, Deng M, Chen S, et al. 25% cell efficiency with integration of passivating contact technology and interdigitated back contact structure on 6 wafers. In: *2019 IEEE 46th Photovoltaic Specialists Conference (PVSC)*. IEEE; 2019:1452-1455. doi:10.1109/PVSC40753.2019.8980596
57. Peibst R, Römer U, Larionova Y, et al. Working principle of carrier selective poly-Si/c-Si junctions: Is tunnelling the whole story? *Sol Energy Mater sol Cells*. 2016;158:60-67. doi:10.1016/j.solmat.2016.05.045
58. Larionova Y, Turcu M, Reiter S, et al. On the recombination behavior of p+-type polysilicon on oxide junctions deposited by different methods on textured and planar surfaces. *Phys Status Solidi a*. 2017;214(8):1700058. doi:10.1002/pssa.201700058
59. Stöhr M, Aprojanz J, Brendel R, Dullweber T. Firing-stable PECVD SiOxNy/n-poly-Si surface passivation for silicon solar cells. *ACS Appl Energy Mater*. 2021;4(5):4646-4653. doi:10.1021/acsaem.1c00265
60. Chen D, Chen Y, Wang Z, et al. 24.58% total area efficiency of screen-printed, large area industrial silicon solar cells with the tunnel oxide passivated contacts (i-TOPCon) design. *Sol Energy Mater sol Cells*. 2020;206:110258. doi:10.1016/j.solmat.2019.110258
61. Merkle A, Seren S, Knauss H, et al. Atmospheric pressure chemical vapor deposition of in-situ doped amorphous silicon layers for passivating contacts. In: *35th European Photovoltaic Solar Energy Conference and Exhibition*. EU PVSEC; 2018:785-791. doi:10.4229/35thEUPVSEC20182018-2DV.3.49
62. Lossen J, Hoß J, Eisert S, et al. Electron beam evaporation of silicon for poly-silicon/SiO_2 passivated contacts. In: *35th European Photovoltaic Solar Energy Conference and Exhibition*. EU PVSEC; 2018:418-421. doi:10.4229/35thEUPVSEC20182018-2CO.10.5
63. Yan D, Cuevas A, Phang SP, Wan Y, Macdonald D. 23% efficient p-type crystalline silicon solar cells with hole-selective passivating contacts based on physical vapor deposition of doped silicon films. *Appl Phys Lett*. 2018;113(6):061603. doi:10.1063/1.5037610
64. Richter A, Müller R, Benick J, et al. Design rules for high-efficiency both-sides-contacted silicon solar cells with balanced charge carrier

transport and recombination losses. *Nat Energy*. 2021;6(4):429-438. doi:10.1038/s41560-021-00805-w

65. Nogay G, Ballif C, Ingenito A, et al. Crystalline silicon solar cells with coannealed electron- and hole-selective SiCx passivating contacts. *IEEE J Photovolt*. 2018;8(6):1478-1485. doi:10.1109/JPHOTOV.2018.2866189
66. Yan D, Cuevas A, Wan Y, Bullock J. Passivating contacts for silicon solar cells based on boron-diffused recrystallized amorphous silicon and thin dielectric interlayers. *Sol Energy Mater sol Cells*. 2016;152:73-79. doi:10.1016/j.solmat.2016.03.033
67. Fogel D. *Encapsulant Characterization and Doped Passivated Contacts for Use in a Luminescent Solar Concentrator*. Colorado School of Mines; 2017. Accessed: Sep. 06, 2021 [Online]. Available: https://mountainscholar.org/handle/11124/171020
68. Stodolny MK, Anker J, Geerligs BLJ, et al. Material properties of LPCVD processed n-type polysilicon passivating contacts and its application in PERPoly industrial bifacial solar cells. *Energy Procedia*. 2017;124:635-642. doi:10.1016/j.egypro.2017.09.250
69. Schnabel M., van de Loo BWH, Nemeth W, et al. Hydrogen passivation of poly-Si/SiO_x contacts for Si solar cells using Al_2O_3 studied with deuterium. *Appl Phys Lett*. 2018;112(20):203901. doi:10.1063/1.5031118
70. Truong TN, Yan D, Samundsett C, et al. Hydrogenation of phosphorus-doped polycrystalline silicon films for passivating contact solar cells. *ACS Appl Mater Interfaces*. 2019;11(5):5554-5560. doi:10.1021/acsami.8b19989
71. Yan D, Cuevas A, Michel JI, et al. Polysilicon passivated junctions: the next technology for silicon solar cells? *Joule*. 2021;5(4):811-828. doi:10.1016/j.joule.2021.02.013
72. Glunz SW, Turan R, Fell A, Feldmann F, Müller R, Kökbudak G. On the determination of the contact resistivity for passivating contacts using 3D simulations. 33rd Eur Photovolt sol Energy Conf Exhib, 2017:242-246. doi:10.4229/EUPVSEC20172017-2AO.4.3
73. Ingenito A, Nogay G, Jeangros Q, et al. A passivating contact for silicon solar cells formed during a single firing thermal annealing. *Nat Energy*. 2018;3(9):800-808. doi:10.1038/s41560-018-0239-4
74. JinkoSolars. High-efficiency N-Type Monocrystalline Silicon Solar Cell Sets New World Record with Highest Conversion Efficiency of 25.4%|JinkoSolar. https://ir.jinkosolar.com/news-releases/news-release-details/jinkosolars-high-efficiency-n-type-monocrystalline-silicon-solar (accessed Oct. 25, 2021).
75. Feldmann F, Nicolai M, Müller R, Reichel C, Hermle M. Optical and electrical characterization of poly-Si/SiO_x contacts and their implications on solar cell design. *Energy Procedia*. 2017;124:31-37. doi:10.1016/j.egypro.2017.09.336
76. Ingenito A, Nogay G, Stuckelberger J, et al. Phosphorous-doped silicon carbide as front-side full-area passivating contact for double-side contacted c-Si solar cells. *IEEE J Photovolt*. 2019;9(2):346-354. doi:10.1109/JPHOTOV.2018.2886234
77. LONGi. LONGi breaks three more world records for solar cell efficiency. https://solarpv-expert.com/2021/06/07/longi-to-break-three-more-world-records-for-solar-cell-efficiency/
78. Horzel J, Bay N, Passig M, Kühnlein H, Shengzhao Y, Verlinden P. Industrial Si solar cells with Cu based plated contacts. In: *2015 IEEE 42nd Photovoltaic Specialist Conference (PVSC)*. IEEE; 2015:1-3. doi:10.1109/PVSC.2015.7355650
79. Ingenito A, Limodio G, Procel P, et al. Silicon solar cell architecture with front selective and rear full area ion-implanted passivating contacts. *Sol RRL*. 2017;1(7):1700040. doi:10.1002/solr.201700040
80. Hollemann C, Haase F, Schäfer S, Krügener J, Brendel R, Peibst R. 26.1%-efficient POLO-IBC cells: quantification of electrical and optical loss mechanisms. *Prog Photovolt*. 2019;27(11):950-958. doi:10.1002/pip.3098
81. Shen H, Omelchenko ST, Jacobs DA, et al. In situ recombination junction between p-Si and TiO2 enables high-efficiency monolithic perovskite/Si tandem cells. *Sci Adv*. 2018;4(12):eaau9711. doi:10.1126/sciadv.aau9711
82. Nogay G, Sahli F, Werner J, et al. 25.1%-efficient monolithic perovskite/silicon tandem solar cell based on a p-type monocrystalline textured silicon wafer and high-temperature passivating contacts. *ACS Energy Lett*. 2019;4(4):844-845. doi:10.1021/acsenergylett.9b00377
83. Shen H, Walter D, Wu Y, et al. Monolithic perovskite/Si tandem solar cells: pathways to over 30% efficiency. *Adv Energy Mater*. 2020;10(13):1902840. doi:10.1002/aenm.201902840
84. Mariotti S, Jäger K, Diederich M, et al. Monolithic perovskite/silicon tandem solar cells fabricated using industrial p-type polycrystalline silicon on oxide/passivated emitter and rear cell Silicon bottom cell technology. *Sol RRL*. 6(4):2101066. doi:10.1002/solr.202101066
85. Battaglia C, de Nicolás SM, de Wolf S, et al. Silicon heterojunction solar cell with passivated hole selective MoOx contact. *Appl Phys Lett*. 2014;104(11):113902. doi:10.1063/1.4868880
86. Kang J, Yang X, Liu W, et al. Electron-selective lithium contacts for crystalline silicon solar cells. *Adv Mater Interfaces*. 8(12):2100015. doi:10.1002/admi.202100015
87. Wang W, He J, Cai L, et al. Solution-processed electron-selective contacts enabling 21.8% efficiency crystalline silicon solar cells. *Sol RRL*. 2020;4(12):2000569. doi:10.1002/solr.202000569
88. He J, Wang W, Cai L, et al. Stable electron-selective contacts for crystalline silicon solar cells enabling efficiency over 21.6%. *Adv Funct Mater*. 2020;30(50):2005554. doi:10.1002/adfm.202005554
89. Yang X, Bi Q, Ali H, Davis K, Schoenfeld WV, Weber K. High-performance TiO_2-based electron-selective contacts for crystalline silicon solar cells. *Adv Mater*. 2016;28(28):5891-5897. doi:10.1002/adma.201600926
90. Wang W, He J, Yan D, et al. 21.3%-efficient n-type silicon solar cell with a full area rear TiO_x/LiF/Al electron-selective contact. *Sol Energy Mater sol Cells*. 2020;206:110291. doi:10.1016/j.solmat.2019.110291
91. Wan Y, Samundsett C, Bullock J, et al. Magnesium fluoride electron-selective contacts for crystalline silicon solar cells. *ACS Appl Mater Interfaces*. 2016;8(23):14671-14677. doi:10.1021/acsami.6b03599
92. Yang X, Liu W, de Bastiani M, et al. Dual-function electron-conductive, hole-blocking titanium nitride contacts for efficient silicon solar cells. *Joule*. 2019;3(5):1314-1327. doi:10.1016/j.joule.2019.03.008
93. Ji W, Allen T, Yang X, Zeng G, De Wolf S, Javey A. Polymeric electron-selective contact for crystalline silicon solar cells with an efficiency exceeding 19%. *ACS Energy Lett*. 2020;5(3):897-902. doi:10.1021/acsenergylett.0c00110
94. Zhang L, Meng L, Cai L, et al. High-performance europium fluoride electron-selective contacts for efficient crystalline silicon solar cells. *Sol RRL*. 5(8):2100057. doi:10.1002/solr.202100057
95. Yang X, Aydin E, Xu H, et al. Tantalum nitride electron-selective contact for crystalline silicon solar cells. *Adv Energy Mater*. 2018;8(20):1800608. doi:10.1002/aenm.201800608
96. Wan Y, Samundsett C, Bullock J, et al. Conductive and stable magnesium oxide electron-selective contacts for efficient silicon solar cells. *Adv Energy Mater*. 2017;7(5):1601863. doi:10.1002/aenm.201601863
97. Wang W, Cai L, Meng L, et al. Cerous fluoride dopant-free electron-selective contact for crystalline silicon solar cells. *Phys Status Solidi RRL – Rapid Res Lett*. 15(12):2100135. doi:10.1002/pssr.202100135
98. Wan Y, Bullock J, Hettick M, et al. Temperature and humidity stable alkali/alkaline-earth metal carbonates as electron heterocontacts for silicon photovoltaics. *Adv Energy Mater*. 2018;8(22):1800743. doi:10.1002/aenm.201800743
99. Wan Y, Samundsett C, Yan D, et al. A magnesium/amorphous silicon passivating contact for n-type crystalline silicon solar cells. *Appl Phys Lett*. 2016;109(11):113901. doi:10.1063/1.4962960

100. Bullock J, Wan Y, Hettick M, et al. Dopant-free partial rear contacts enabling 23% silicon solar cells. *Adv Energy Mater*. 2019;9(9):1803367. doi:10.1002/aenm.201803367
101. Allen TG, Bullock J, Zheng P, et al. Calcium contacts to n-type crystalline silicon solar cells: Calcium contacts to n-type crystalline silicon solar cells. *Prog Photovolt Res Appl*. 2017;25(7):636-644. doi:10.1002/pip.2838
102. Bullock J, Zheng P, Jeangros Q, et al. Lithium fluoride based electron contacts for high efficiency n-type crystalline silicon solar cells. *Adv Energy Mater*. 2016;6(14):1600241. doi:10.1002/aenm.201600241
103. Allen TG, Bullock J, Jeangros Q, et al. A low resistance calcium/reduced titania passivated contact for high efficiency crystalline silicon solar cells. *Adv Energy Mater*. 2017;7(12):1602606. doi:10.1002/aenm.201602606
104. Dréon J, Jeangros Q, Cattin J, et al. 23.5%-efficient silicon heterojunction silicon solar cell using molybdenum oxide as hole-selective contact. *Nano Energy*. 2020;70:104495. doi:10.1016/j.nanoen.2020.104495
105. Yang X, Xu H, Liu W, et al. Atomic layer deposition of vanadium oxide as hole-selective contact for crystalline silicon solar cells. *Adv Electron Mater*. 2020;6(8):2000467. doi:10.1002/aelm.202000467
106. Matsui T, Bivour M, Hermle M, Sai H. Atomic-layer-deposited TiO_x nanolayers function as efficient hole-selective passivating contacts in silicon solar cells. *ACS Appl Mater Interfaces*. 2020;12(44):49777-49785. doi:10.1021/acsami.0c14239
107. Halbich MU, Zielke D, Gogolin R, Sauer-Stieglitz R, Lövenich W, Schmidt J. Improved surface passivation and reduced parasitic absorption in PEDOT:PSS/c-Si heterojunction solar cells through the admixture of sorbitol. *Sci Rep*. 2019;9(1):9775. doi:10.1038/s41598-019-46280-y
108. Zielke D, Gogolin R, Halbich MU, et al. Large-area PEDOT:PSS/c-Si heterojunction solar cells with screen-printed metal contacts. *Sol RRL*. 2018;2(3):1700191. doi:10.1002/solr.201700191
109. Bullock J, Samundsett C, Cuevas A, Yan D, Wan Y, Allen T. Proof-of-concept p-type silicon solar cells with molybdenum oxide local rear contacts. *IEEE J Photovolt*. 2015;5(6):1591-1594. doi:10.1109/JPHOTOV.2015.2478026
110. Lin W, Wu W, Liu Z, et al. Chromium trioxide hole-selective heterocontacts for silicon solar cells. *ACS Appl Mater Interfaces*. 2018;10(16):13645-13651. doi:10.1021/acsami.8b02878
111. Masmitjà G, Gerling LG, Ortega P, et al. V_2O_x-based hole-selective contacts for c-Si interdigitated back-contacted solar cells. *J Mater Chem a*. 2017;5(19):9182-9189. doi:10.1039/C7TA01959A
112. Wu W, Lin W, Zhong S, et al. 22% efficient dopant-free interdigitated back contact silicon solar cells, 2018:040025. doi:10.1063/1.5049288
113. Bullock J, Wan Y, Xu Z, et al. Stable dopant-free asymmetric heterocontact silicon solar cells with efficiencies above 20%. *ACS Energy Lett*. 2018;3(3):508-513. doi:10.1021/acsenergylett.7b01279
114. Li F, Sun Z, Zhou Y, et al. Lithography-free and dopant-free back-contact silicon heterojunction solar cells with solution-processed TiO_2 as the efficient electron selective layer. *Sol Energy Mater sol Cells*. 2019;203:110196. doi:10.1016/j.solmat.2019.110196
115. Reichel C, Würfel U, Winkler K, et al. Electron-selective contacts via ultra-thin organic interface dipoles for silicon organic heterojunction solar cells. *J Appl Phys*. 2018;123(2):024505. doi:10.1063/1.5010937
116. Bullock J, Hettick M, Geissbühler J, et al. Efficient silicon solar cells with dopant-free asymmetric heterocontacts. *Nat Energy*. 2016;1(3):15031. doi:10.1038/nenergy.2015.31
117. Wu W, Lin W, Zhong S, et al. Dopant-free back-contacted silicon solar cells with an efficiency of 22.1%. *Phys Status Solidi RRL – Rapid Res Lett*. 2020;14(4):1900688. doi:10.1002/pssr.201900688
118. Lin W, Dréon J, Zhong S, et al. Dopant-free bifacial silicon solar cells. *Sol RRL*. 2021;5(5):2000771. doi:10.1002/solr.202000771

How to cite this article: Yan D, Cuevas A, Stuckelberger J, et al. Silicon solar cells with passivating contacts: Classification and performance. *Prog Photovolt Res Appl*. 2022;1-17. doi:10.1002/pip.3574